Journal of Medical Sciences

ISSN 1682-4474

science alert

ANSInet
an open access publisher
http://ansinet.com

Research Paper

JMS (ISSN 1682-4474) is an International, peer-reviewed scientific journal that publishes original article in experimental & clinical medicine and related disciplines such as molecular biology, biochemistry, genetics, biophysics, bio-and medical technology. JMS is issued four times per year on paper and in electronic format.

For further information about this article or if you need reprints, please contact:

A. Prabhu Britto
Center for Medical Electronics,
Department of Electronics and Communication Engineering,
Anna University,
Chennai 600 025, India

J. Med. Sci., 6 (1): 117-124
January-March, 2006

Segmentation of Chromosome Spread Images using Discrete Cosine Transform Based Gradient Vector Flow Active Contours: An Analysis

[1]A. Prabhu Britto and [2]G. Ravindran

In this study, segmentation of chromosome images is done using Discrete Cosine Transform (DCT) based Gradient Vector Flow (GVF) active contours. The parameters used in the active contour formulation have been characterized standardized. The standardized values of the parameters are used in this study. The segmentation errors have been quantified. The analysis of the error quantification yields valuable insight into the performance of the DCT based GVF active contours as a segmentation tool for chromosome spread images.

Key words: Chromosome, segmentation, gradient vector flow active contours, error quantification, performance

ANSInet
Asian Network for Scientific Information

[1]Center for Medical Electronics,
Department of Electronics and Communication Engineering,
[2]Faculty of Information and Communication Engineering,
Anna University, Chennai 600 025, India

INTRODUCTION

This research used characterized Discrete Cosine Transform (DCT) based Gradient Vector Flow (GVF) active contours[1] for segmentation of chromosome spread images. The main advantage of using these characterized parameters is that they have already been standardized and can be used for segmentation of any similar class of chromosome spread images[2]. The segmentation error is the difference between the length of the axis of the chromosome and the length of the axis of the contour in both the major and minor axes. Segmentation has been performed on 318 images drawn from three independent datasets and the segmentation errors have been quantified. A study of the segmentation error and the segmentation method yields valuable insight into the performance of the DCT based GVF active contours as a segmentation tool for chromosome spread images and also yields directions for future study to improve the efficiency of the technique.

CHROMOSOME IMAGES

The chromosome spread images are obtained using the following general procedure. About 5 mL of blood is removed from the patient. If a fetus is being karyotyped, amniotic fluid is removed from the amniotic sac which surrounds the fetus during development. This is done with the aid of a large syringe and ultrasound picturing. There are cells which have come off the fetus in this fluid. The white blood cells are removed from the blood or the living cells are removed from the amniotic fluid. These cells are then cultured in a medium in which they undergo mitosis. Mitosis is stopped at metaphase using chemicals. The cells are then placed onto a slide and spread out. They are viewed under a microscope which is specially adapted with a camera to take a picture of the chromosomes from one of the cells[3].

Hence, the chromosomes in a spread image have variations in shape caused due to bending effects, variations due to overlaps, variations due to illumination and device dependencies. This causes difficulties in segmenting the chromosome images as the segmenting algorithm or technique needs to be retrained often. Therefore, a special class of deformable curves called Gradient vector flow active contours is chosen to perform good and efficient segmentation of chromosome spread images under such difficulties caused by so much of variation.

GRADIENT VECTOR FLOW (GVF) ACTIVE CONTOURS

Gradient Vector Flow (GVF) active contours use gradient vector flow fields obtained by solving a vector diffusion equation that diffuses the gradient vectors of a gray-level edge map computed from the image. The GVF active contour model cannot be written as the negative gradient of a potential function. Hence it is directly specified from a dynamic force equation, instead of the standard energy minimization network.

The external forces arising out of GVF fields are non-conservative forces as they cannot be written as gradients of scalar potential functions. The usage of non-conservative forces as external forces show improved performance of gradient vector flow field active contours compared to traditional energy minimizing active contours[4,5].

The GVF field points towards the object boundary when very near to the boundary, but varies smoothly over homogeneous image regions extending to the image border. Hence the GVF field can capture an active contour from long range from either side of the object boundary and can force it into the object boundary. The GVF active contour model thus has a large capture range and is insensitive to the initialization of the contour. Hence the contour initialization is flexible.

The gradient vectors are normal to the boundary surface but by combining Laplacian and Gradient the result is not the normal vectors to the boundary surface. As a result of this, the GVF field yields vectors that point into boundary concavities so that the active contour is driven through the concavities. Information regarding whether the initial contour should expand or contract need not be given to the GVF active contour model. The GVF is very useful when there are boundary gaps, because it preserves the perceptual edge property of active contours[5,6].

The GVF field is defined as the equilibrium solution to the following vector diffusion equation:

$$u_t = g(|\nabla f|)\nabla^2 u - h(|\nabla f|)(u - \nabla f) \quad (1a)$$

$$u(x, 0) = \nabla f(x) \quad (1b)$$

Where, u_t denotes the partial derivative of u(x,t) with respect to t, ∇^2 is the Laplacian operator (applied to each spatial component of u separately) and f is an edge map that has a higher value at the desired object boundary.

The functions in g and h control the amount of diffusion in GVF. In Eq. 1, $g(|\nabla f|)\nabla^2 u$ produces a smoothly varying vector field and hence called as the smoothing term, while $h(|\nabla f|)(u-\nabla f)$ encourages the vector field u to be close to ∇f computed from the image data and hence called as the data term. The weighting functions $g(\cdot)$ and $h(\cdot)$ apply to the smoothing and data terms respectively and they are chosen[5] as $g(|\nabla f|) = \mu$ and $h(|\nabla f|) = |\nabla f|^2$. $g(\cdot)$ is constant here and smoothing occurs everywhere, while $h(\cdot)$ grows larger near strong edges and dominates at boundaries.

Hence, the Gradient Vector Flow field is defined as the vector field $v(x,y)=[u(x,y),v(x,y)]$ that minimizes the energy functional:

$$\varepsilon = \int\int \mu(u_x^2+u_y^2+v_x^2+v_y^2)+|\nabla f|^2 |v-\nabla f|^2 \, dxdy \qquad (2)$$

The effect of this variational formulation is that the result is made smooth when there is no data.

When the gradient of the edge map is large, it keeps the external field nearly equal to the gradient, but keeps field to be slowly varying in homogeneous regions where the gradient of the edge map is small, i.e., the gradient of an edge map ∇f has vectors point toward the edges, which are normal to the edges at the edges and have magnitudes only in the immediate vicinity of the edges and in homogeneous regions ∇f is nearly zero. μ is a regularization parameter that governs the tradeoff between the first and the second term in the integrand in Eq. 2. The solution of Eq. 2 can be done using the Calculus of Variations and further by treating u and v as functions of time, solving them as generalized diffusion equations.

DISCRETE COSINE TRANSFORM (DCT) BASED GVF ACTIVE CONTOURS

The transform of an Image yields more insight into the properties of the image. The Discrete Cosine Transform has excellent energy compaction. Hence, the Discrete Cosine Transform promises better description of the image properties. The Discrete Cosine Transform is embedded into the GVF Active Contours. When the image property description is significantly low, this helps the contour model to give significantly better performance by utilizing the energy compaction property of the DCT.

The 2D DCT is defined as :

$$C(u,v) = \alpha(u)\alpha(v)\sum_{x=0}^{N-1}\sum_{y=0}^{N-1} f(x,y)\cos\left[\frac{(2x+1)u\pi}{2N}\right]\cos\left[\frac{(2y+1)v\pi}{2N}\right] \qquad (3)$$

The local contrast of the Image at the given pixel location (k,l) is given by

$$P(k,l) = \frac{\sum_{t=1}^{2(2n+1)-1} w_t E_t}{d_{00}} \qquad (4)$$

where,

$$E_t = \frac{\sum_{u+v=t} |d_{u,v}|}{N} \qquad (5)$$

and

$$N = \begin{cases} t+1 & t<2n+1 \\ 2(2n+1)-t & t\geq 2n+1 \end{cases} \qquad (6)$$

Here, w_t denotes the weights used to select the DCT coefficients. The local contrast P(k,l) is then used to generate a DCT contrast enhanced Image[7], which is then subject to selective segmentation by the energy compact gradient vector flow active contour model using Eq. 2.

MATERIALS AND METHODS

The chromosome metaphase image (at 72 pixels per inch resolution) provided by Prof. Ken Castleman and Prof. Qiang Wu (Advanced Digital Imaging Research, Texas) was taken and preprocessed. Insignificant and unnecessary regions in the image were removed interactively.

Interactive selection of the chromosome of interest was done by selecting a few points around the chromosome that formed the vertices of a polygon. On constructing the perimeter of the polygon, seed points for the initial contour were determined automatically by periodically selecting every third pixel along the perimeter of the polygon.

The GVF deformable curve was then allowed to deform until it converged to the chromosome boundary. The optimum parameters for the deformable curve with respect to the Chromosome images were determined by tabulated studies.

The image was made to undergo minimal preprocessing so as to achieve the goal of boundary mapping in chromosome images with very weak edges.

The DCT based GVF Active contour is governed by the following parameters, namely, σ, μ, α, β and κ. σ determines the Gaussian filtering that is applied to the image to generate the external field.

Larger value of σ will cause the boundaries to become blurry and distorted and can also cause a shift in the boundary location. However, large values of σ are necessary to increase the capture range of the active contour. μ is a regularization parameter and requires a higher value in the presence of noise in the image. α determines the tension of the active contour and β determines the rigidity of the contour. The tension keeps the active contour contracted and the rigidity keeps it

smooth. α and β may also take on value zero implying that the influence of the respective tension and rigidity terms in the diffusion equation is low. κ is the external force weight that determines the strength of the external field that is applied. The iterations were set suitably.

RESULTS AND DISCUSSION

Characterization of parameters of the DCT based GVF active contour segmentation scheme has yielded the values of σ = 0.25, μ = 0.075, α = 0, β = 0 and κ = 0.625 as characterized parameter values[1]. Standardization experiments have established that the characterized parameter values are indeed standardized and can be used for segmenting chromosome spread images from any dataset[2]. Therefore, chromosome images from three independent datasets.

Three hundred and eighteen images from the three datasets were segmented using DCT based GVF active contours. A sample image, its DCT based GVF field and its corresponding segmented image are shown Fig. 1a-c.

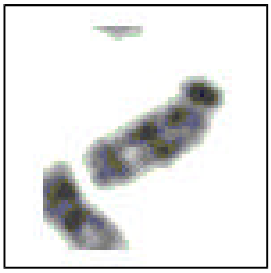

Fig. 1a: Sample chromosome image

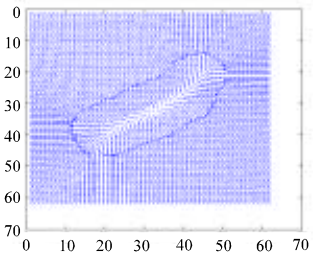

Fig. 1b: DCT based GVF field of Fig. 1a

Fig. 1c: Segmented output image of Fig. 1a

Though the segmentation appears very accurate to the naked eye, still there is a very small error in segmentation, which can be measured as a difference between the lengths of the corresponding axes in the original image and the contoured image along the major and minor axes. Table 1 indicates the segmentation error for the 318 samples.

Table 1: Segmentation error for 318 samples from 3 datasets

Sample No.	Major axis error (original length-contour length) (pixels)	Minor axis error (original length-contour length) (pixels)
1	-0.99234	-0.77586
2	-0.92236	-1.46862
3	-1.22054	-1.42285
4	-0.50117	-1.52401
5	-0.79909	-1.30565
6	-1.22146	-1.42426
7	-1.60087	-1.22658
8	-1.10032	-1.47955
9	-1.34776	-1.48373
10	-1.23882	-1.44197
11	-0.50507	-1.44064
12	-0.96458	-1.44485
13	-0.74198	-1.28465
14	-1.11022	-1.44755
15	-1.54751	-1.21376
16	-1.07456	-1.06164
17	-1.18620	-1.40481
18	-0.72746	-1.26487
19	-0.87464	-0.99237
20	-0.98865	-1.60270
21	-1.36978	-1.39478
22	-1.17438	-1.55330
23	-1.15443	-1.66572
24	-1.08046	-0.98045
25	-0.43939	-1.34720
26	-0.89802	-1.20665
27	-0.83986	-1.51281
28	-1.19226	-1.27562
29	-0.91641	-1.22666
30	-1.19527	-1.21299
31	-1.07868	-1.37991
32	-1.30690	-1.58629
33	-1.04222	-1.50022
34	-1.07693	-1.30267
35	-1.19339	-1.34228
36	-0.19700	-0.99148
37	-1.00575	-1.38379
38	-1.27024	-1.26217
39	-1.19052	-1.59091
40	-1.57068	-1.34149
41	-0.06525	-1.28828
42	-1.41057	-1.50256
43	-0.95857	-1.33091
44	-1.14472	-1.57406
45	-1.14955	-0.80863
46	-1.44815	-0.92282
47	-0.73334	-1.21153
48	-0.75248	-1.10831
49	-0.83161	-1.13684
50	-1.44550	-1.20030
51	-0.43732	-0.94117
52	-1.18084	-0.88306
53	-1.10051	-0.98233

Table 1: Continue

Sample No.	Major axis error (original length-contour length) (pixels)	Minor axis error (original length-contour length) (pixels)
54	-0.84817	-0.81311
55	-0.85195	-0.85861
56	-1.42601	-1.36767
57	-1.08792	-1.25818
58	-1.00787	-1.57067
59	-1.14183	-1.24749
60	-1.05512	-1.23353
61	-1.04553	-1.47289
62	-1.24598	-1.17803
63	-1.24591	-0.94797
64	-1.09302	-0.60602
65	-1.47522	-0.65208
66	-1.64811	-1.21276
67	-1.35375	-1.02046
68	-1.53547	-1.34357
69	-0.81989	-1.38108
70	-1.52447	-1.52537
71	-1.11803	-1.05693
72	-1.17289	-1.08357
73	-1.44782	-1.46856
74	-1.39830	-0.82576
75	-1.15490	-1.76725
76	-1.67470	-1.82524
77	-0.81155	-1.49077
78	-1.05548	-1.12106
79	-1.46508	-1.59271
80	-0.92984	-1.44742
81	-1.17446	-1.41412
82	-1.31850	-1.85090
83	-1.28303	-1.82369
84	-1.70544	-1.80314
85	-1.12819	-1.78943
86	-1.30676	-1.81068
87	-1.68656	-1.76121
88	-1.54859	-1.83839
89	-1.78451	-1.41870
90	-1.50161	-1.56242
91	-1.75045	-1.68973
92	-1.71437	-1.49166
93	-1.29189	-1.61142
94	-1.11535	-1.43806
95	-1.16706	-0.84660
96	-0.35002	-1.26907
97	-1.65977	-1.44606
98	-1.32436	-1.44325
99	-0.83952	-1.30286
100	-1.46343	-1.49125
101	-1.34706	-1.44058
102	-0.77316	-0.93570
103	-0.92317	-1.43493
104	-0.82944	-1.52511
105	-1.09132	-1.24394
106	-1.71227	-1.25855
107	-0.65384	-1.25014
108	-0.99551	-1.43557
109	-1.55370	-1.12406
110	-1.25816	-1.59663
111	-1.39701	-1.57356
112	-1.34014	-1.60741
113	-1.17887	-1.57955
114	-1.46369	-1.85403
115	-1.83897	-1.15738
116	-1.54852	-1.64479
117	-1.07914	-1.78763
118	-1.04431	-1.37157
119	-0.81271	-1.74084
120	-1.46568	-1.27865

Table 1: Continue

Sample No.	Major axis error (original length-contour length) (pixels)	Minor axis error (original length-contour length) (pixels)
121	-1.15892	-1.45032
122	-1.59849	-1.62836
123	-1.43299	-1.53496
124	-1.40452	-1.65714
125	-1.34607	-1.78251
126	-1.36388	-1.65470
127	-1.29578	-1.56038
128	-1.75492	-1.49270
129	-0.51893	-1.02551
130	-1.52641	-1.32845
131	-0.98419	-0.88066
132	-1.25835	-1.62751
133	-1.31813	-1.28318
134	-1.22756	-1.79120
135	-1.39908	-1.63411
136	-1.50758	-1.69494
137	-1.62147	-1.80409
138	-1.24531	-1.70962
139	-1.42302	-1.66979
140	-1.80824	-1.48837
141	-1.39578	-1.60001
142	-1.46443	-1.86732
143	-1.25127	-1.33970
144	-1.22927	-1.49507
145	-1.47127	-1.16732
146	-0.77176	-1.47202
147	-1.52120	-1.47896
148	-1.78376	-1.77441
149	-1.23595	-1.84757
150	-1.28518	-1.77467
151	-1.67906	-1.83505
152	-1.64093	-1.70609
153	-1.54124	-1.77961
154	-0.87704	-1.71266
155	-1.56672	-1.60876
156	-1.60235	-1.58664
157	-1.62993	-1.68170
158	-1.39020	-1.52869
159	-1.30491	-1.38873
160	-1.45918	-1.76656
161	-1.21411	-1.37777
162	-1.31448	-1.66411
163	-1.63016	-1.37270
164	-1.36548	-1.42156
165	-1.70219	-1.59919
166	-1.41931	-1.64704
167	-1.65577	-1.55406
168	-1.05519	-1.64028
169	-1.61059	-1.32320
170	-1.47530	-1.46667
171	-1.62097	-1.76199
172	-1.50341	-1.50896
173	-1.22407	-1.49762
174	-1.48875	-1.75695
175	-1.53238	-1.74492
176	-1.37271	-1.79914
177	-1.32930	-1.56507
178	-1.38051	-1.38384
179	-1.76723	-1.65650
180	-1.02523	-1.72864
181	-1.54005	-1.65639
182	-1.72919	-1.15239
183	-1.20443	-1.51663
184	-0.99931	-1.78782
185	-1.30143	-1.71629
186	-1.62004	-1.61166

Table 1: Continue

Sample No.	Major axis error (original length-contour length) (pixels)	Minor axis error (original length-contour length) (pixels)
187	-1.61173	-1.70276
188	-0.94217	-1.37329
189	-1.57811	-1.56130
190	-1.26361	-1.43489
191	-1.28947	-1.48325
192	-1.55792	-1.79845
193	-1.20496	-1.26730
194	-1.45997	-1.78202
195	-1.48458	-1.77118
196	-1.05893	-1.36052
197	-1.54709	-1.75364
198	-1.48502	-1.73452
199	-1.60663	-1.43784
200	-1.40431	-1.50349
201	-1.70940	-1.80180
202	-1.62712	-1.64777
203	-1.58439	-1.52570
204	-1.52230	-1.54799
205	-1.58271	-1.74528
206	-1.43155	-1.82118
207	-1.49083	-1.57735
208	-1.67561	-1.80151
209	-1.82834	-1.34893
210	-1.68152	-1.45958
211	-1.45422	-1.50967
212	-1.66564	-1.57033
213	-1.75264	-1.51341
214	-1.35870	-1.44900
215	-1.48712	-1.63543
216	-1.68667	-1.27302
217	-1.75286	-1.64936
218	-1.90007	-1.68043
219	-1.75245	-1.64335
220	-1.15253	-1.67732
221	-1.71058	-1.54840
222	-1.77340	-1.37673
223	-1.68952	-1.39025
224	-1.27634	-1.64743
225	-1.36688	-1.71029
226	-1.26568	-1.45783
227	-1.68079	-1.64198
228	-1.60843	-1.43617
229	-1.01098	-1.24097
230	-1.17909	-1.59647
231	-1.14902	-1.59096
232	-1.73711	-1.16556
233	-1.35609	-1.59542
234	-1.80709	-1.37058
235	-1.46277	-1.06366
236	-1.03423	-1.68603
237	-1.43354	-1.10977
238	-1.68230	-1.37330
239	-1.02910	-1.61454
240	-1.23612	-1.60362
241	-1.06309	-1.41744
242	-1.38347	-1.33055
243	-1.96348	-1.27382
244	-1.32787	-0.99786
245	-1.15841	-1.13018
246	-1.15632	-0.79230
247	-0.62158	-0.98635
248	0.095851	-1.08807
249	-1.32411	-1.10890
250	-1.42063	-0.69022
251	-1.02292	-1.51586
252	-0.53597	-1.08469

Table 1: Continue

Sample No.	Major axis error (original length-contour length) (pixels)	Minor axis error (original length-contour length) (pixels)
253	-0.93526	-1.35863
254	-1.12979	-1.32887
255	-1.32098	-1.39625
256	-1.59181	-1.62762
257	-1.08802	-1.67128
258	-1.35797	-1.76089
259	-1.57749	-0.87660
260	-1.47635	-1.66279
261	-1.64221	-1.60452
262	-1.72534	-1.64434
263	-1.30636	-1.26789
264	-1.44442	-1.34894
265	-1.72459	-1.45015
266	-1.33014	-1.28475
267	-1.22127	-1.49620
268	-1.44321	-1.49924
269	-0.44263	-0.88506
270	-1.51196	-1.26339
271	-0.55577	-1.34103
272	-1.12876	-1.37085
273	-0.45910	-1.02262
274	-1.79495	-0.47482
275	-0.75910	-0.92719
276	-0.80834	-1.10319
277	-0.67699	-0.42107
278	-1.56579	-1.64864
279	-0.77940	-1.12020
280	-0.88227	-1.84570
281	-0.60852	-0.76666
282	-1.09408	-0.86361
283	-0.05593	-1.07659
284	-1.34116	-0.54712
285	-0.76100	-1.10153
286	-0.51221	-1.34777
287	-1.04211	-1.06338
288	-1.28801	-1.41891
289	-0.90978	-1.26579
290	-1.09583	-1.36193
291	-1.58498	-1.20230
292	-0.68618	-1.06145
293	-0.52599	-1.03633
294	-1.25896	-0.55402
295	-1.07661	-1.43257
296	-0.88606	-1.54889
297	-1.69623	-1.07352
298	-1.01829	-1.06702
299	-0.54430	-1.06371
300	-1.04393	-0.78641
301	-1.28628	-1.44046
302	-1.10610	-1.31402
303	-1.34172	-1.61017
304	-1.36776	-1.35632
305	-1.40992	-1.67894
306	-1.19584	-1.45892
307	-1.56708	-1.46632
308	-0.99464	-1.13423
309	-0.75426	-1.14705
310	-1.05052	-1.33393
311	-1.63924	-1.12882
312	-0.67669	-1.22881
313	-0.95541	-1.27993
314	-1.53796	-1.11813
315	-0.85000	-1.23130
316	-1.56739	-1.68077
317	-0.92468	-1.44381
318	-0.83829	-1.15258

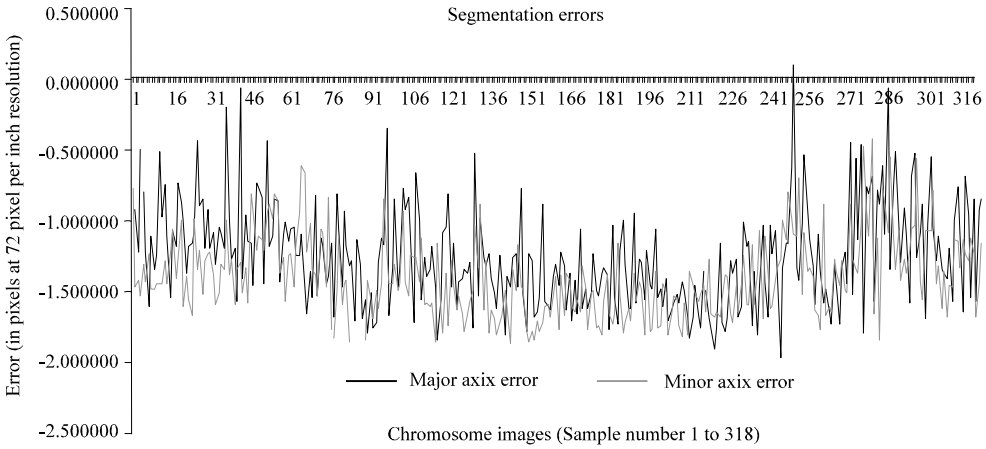

Fig. 2: Segmentation errors obtained while segmenting 318 sample chromosome images from 3 independent datasets

From Fig. 2, it is observed that the major axis error oscillates more than the minor axis error. This may be due the fact that the maximum radius along the major axis of the chromosome is 64.873797 and the minimum radius along the major axis is 11.489264, while the maximum and minimum lengths of the chromosome alone the minor axis are only 25.821964 and 7.354900. The ratio of the maxima to the minima along the major axis is approximately 5.646471 while the same ratio along the minor axis is only 3.510851. Hence the segmentation error along the minor axis may seem to manifest less oscillation, but given the less ratio of the maximum to minimum length as 3.510851 compared to 5.646471 along the major axis, it can be inferred that the oscillations of the error along the major and the minor axis oscillate proportionally. This lends support to the fact that the tension and rigidity parameters that assume a constant value in the DCT based GVF Active Contour formulation enforce a circular iterative effect on the initial contour, forcing it to converge circularly on the chromosome image, irrespective of the size of the chromosome or ratio of the major axis length to the minor axis length.

Also, we find from Fig. 2 that the error varies only between 0.055934 and 1.963482, when segmented with DCT based GVF Active Contours with parameter values of $\sigma = 0.25$, $\mu = 0.075$, $\alpha = 0$, $\beta = 0$ and $\kappa = 0.625$ and subjected to limited preprocessing and enhancement using only median filtering, adaptive histogram equalization, averaging and graylevel adjustment using built-in Matlab functions.

It is found that the characterization and the preprocessing and enhancement requirements play a vital role in the successful segmentation of chromosome spread images using DCT based GVF active contours. To extend this technique for universal segmentation of chromosome spread images, retraining by repeated characterization would defeat the aim of universal segmentation itself. Since preprocessing and enhancement requirements also play a vital role, concentration can be exercised on them to reduce the segmentation error to less than one pixel that is found in characterized segmented chromosome image samples, which is acceptable as the contour iterative step size is one pixel and the contour thickness is also one pixel wide. Too much of enhancement and preprocessing would destroy the build up of the effective gradient between the background and the image boundary which is essential for the effective convergence of the DCT based GVF active contour. Therefore, optimum enhancement and preprocessing by trial-and-error method is sufficient for good convergence of the DCT based GVF active contour with acceptable segmentation error less than one pixel.

This makes the DCT based GVF Active Contour accompanied with optimum preprocessing and enhancement, an efficient segmentation tool for any chromosome, provided that the DCT based GVF Active Contour is characterized with chromosomes that are same or similar to the chromosome of interest, to achieve best results.

CONCLUSIONS

Therefore, the DCT based GVF active contours are hence established as an efficient tool for chromosome image segmentation independent of the dataset from which the images are obtained.

ACKNOWLEDGMENTS

The authors extend their heartfelt thanks to Dr. Michael Difilippantonio, Staff Scientist at the Section of Cancer Genomics, Genetics Branch/CCR/NCI/ NIH,

Bethesda MD; Prof. Ekaterina Detcheva at the Artificial Intelligence Department, Institute of Mathematics and Informatics, Sofia, Bulgaria; Prof. Ken Castleman and Prof. Qiang Wu, from Advanced Digital Imaging Research, Texas and Wisconsin State Laboratory of Hygiene-http://worms.zoology.wisc.edu/zooweb/Phelps/karyotype.html for their help in providing chromosome spread images.

REFERENCES

1. Britto, A.P. and G. Ravindran, 2005. Boundary mapping of chromosome spread images using optimal set of parameter values in discrete cosine transform based gradient vector flow active contours. J. Applied Sci., (Accepted).
2. Britto, A.P. and G. Ravindran, 2005. Evaluation of standardization of curve evolution based boundary mapping technique for chromosome spread images. J. Inform. Technol., (Accepted).
3. http://home.earthlink.net/~heinabilene/karyotypes/karyoty.htm
4. Xu, C. and J.L. Prince, 2000. Gradient Vector Flow Deformable Models. In: Handbook of Medical Imaging, Academic Press, pp: 159-169.
5. Xu, C. and J.L. Prince, 1998. Snakes, shapes and gradient vector flow. IEEE Transactions on Image Processing, 7: 359-369.
6. Kass, M., A. Witkin and D. Terzopoulos, 1987. Snakes: Active contour models. Intl. J. Comp. Vision, 1: 321-331.
7. Jinshan, T. and S.T. Acton, 2004. A DCT based gradient vector flow snake for object boundary detection. 6th IEEE Southwest Symposium on Image Analysis and Interpretation, pp: 157-161.